

HEAT TRANSFER ENHANCEMENT BY SINUSOIDAL WAVY TAPE INSERT IN TWO-PASS RIBBED CHANNELS

by

Jiang WEI, Ziyue MEI, Fan WU, Youmin HOU, and Danmei XIE*

School of Power and Mechanical Engineering, Wuhan University, Wuhan, China

Original scientific paper

<https://doi.org/10.2298/TSCI211226064J>

The turbine inlet temperature is one of the most critical parameter that determines the thermal efficiency and thrust-weight ratio of the gas turbine. However, the higher gas turbine inlet temperature significantly increases the thermal stress on the blade, which necessitates effective cooling strategy to reduce the blade temperature. In this study, a united blade cooling strategy was developed by adopting a two-pass ribbed cooling channel with wavy tape for the reason that ribs are near-wall turbulence promoters while the wavy tape is core-region promoter with relatively lower pressure-drop penalty. Ribs and wavy tape may complement each other in the cooling channel. The synergistic effect of the combined near-wall and core-region heat transfer promoter was numerically studied for Reynolds numbers from 6000 to 30000. Two key geometrical factors, namely rib to wave crest phase shift and relative wave amplitude, have significant effect on the thermal performance. The results demonstrate that wavy tape with different phase shift configurations can eliminate the lower heat transfer areas and produce more uniform heat transfer. The 0° phase shift achieved best overall thermal performance, which provided 1.07-1.08 times the flat tape heat transfer enhancement with 1.09-1.11 times the pressure drop penalty. The better heat performance is due to the secondary flow induced by wavy tape, which enhances the fluid mixing between near-wall and core-region.

Key words: heat transfer enhancement, wavy tape, 90° ribs, two-pass channel

Introduction

Gas turbine is one of the most important power sources that are widely used in various industrial applications, such as power plants, air crafts, and ships. With the development of gas turbine technologies, the inlet temperature of the gas turbine has been increased significantly to enhance the thermal efficiency. As the turbine inlet temperature is far beyond the allowable metal temperatures, advanced cooling methods are necessary to avoid the failure of gas turbine blades, especially during the long-term operation. As one of the most effective cooling techniques, the internal blade cooling is on the basis of convective heat transfer with its intensity depending on the velocity and the turbulence level of the coolant. With the expectation of not increasing coolant usage too much, some united and complicated cooling strategies should be developed to achieve higher turbulence level while maintain relatively low pressure-drop penalty. Traditionally, turbulence promoters were used inside cooling passages to enhance the heat transfer of the internal surface on the turbine blade. Among different turbulence promoters, the straight rib is attractive in principle because they are easy to process, and can increase the

* Corresponding author, e-mail: dmxie@whu.edu.cn

heating surface and structural strength meanwhile. Heat transfer enhancement by ribbed wall has been largely studied numerically and experimentally in the past, with the main purpose of establishing basic optimal geometry parameters for better overall thermal performance. As pioneering studies, Han *et al.* [1-4] conducted systematic experiments to investigate the effects of rib configuration (*e.g.*, rib height, spacing, angle of attack) and flow Reynolds number on the average heat transfer and pressure drop in the fully developed region of uniformly heated square channel [1, 2] and developed ribbed channels with different entrance aspect ratios [3, 4]. Besides, the effect of rib orientation, rib angle and sharp 180° turn on the local heat and mass transfer from two- or three-pass square channels were also been reported [5-7]. Recently, some measurements of heat transfer rate have been conducted on the rotating condition. The attentions have been paid to the effect of rib height and channel orientation on heat transfer at high rotation numbers [8, 9]. The shape of ribs can affect the thermal performance besides the basic geometry parameters of traditional straight rib. Some new morphology of ribs, such as semi-attached rib [10], crescent rib [11], V-shape rib [12], W-shape rib [13], semicircular rib [14], and truncated rib [15], were found to outperform the traditional straight rib. The graded baffles, which have up- or down-graded height along the channel length, were demonstrated with decreasing friction factor [16]. However, the ribs mainly disturb the flow close to the internal surface, so the mixing between near-wall and core-region is not so intensive.

In searching for core-region turbulence promoter, it was noticed that twisted tapes can boost the mass transfer between near-wall and core-region and thus remove the heat accumulated near the wall. In the early application [17], the twisted tape was employed in tube as swirl flow generator for heat transfer enhancement. Recently, Promvong and Eiamsa-Ard [18] combined the twisted tape with conical rings in the tube, and reported 4-10% increases in Nusselt number and 4-8% increase in efficiency compared to that with conical-ring alone. Besides, the effect of twisted tape on heat transfer performance enhancement was further confirmed in the spirally grooved tube [19]. If larger Nusselt number is targeted, the broken twisted tape [20] maybe a good choice at the cost of larger friction factors. Previous studies mainly focused on twisted tape insert in tubes, but twisted tape does not fit into the rectangular channel with only one or two sides ribbed.

Similar to the twisted tape, the use of wavy channel wall has been suggested in literature to boost the heat transfer performance as passive scheme. Macroscopic mixing and augment of local heat transfer can be observed in a channel bound by two wavy walls [21]. The experiment of Kuhn and von Rohr [22] further confirmed the mixed convection on a heated wavy surface and found an increase of momentum transport near the heated surface. What's more, the effect of wavy wall is not limited by the small turbulence promoters on the wall surface [23] or the dimension of the channels [24]. Besides, the numerical results [25] indicate that the wavy wall can achieve heat transfer augmented with a relatively small pressure drop penalty. Recently, Zhu *et al.* [26, 27] found wavy tape insert may achieve similar effect as the twisted tape did in the tube. Bhattacharyya's [28] experiment reported that wavy-tape inserts can augment the heat transfer by up to 67% higher than smooth tubes, which may find its application in designing efficient solar air heaters [27] and heat exchangers [29]. Some more structurally complicated wavy tape, such as center-tapered wavy tape insert [30], was found to achieve better overall performance.

Despite extensive progress, there is still a lack of measures to effectively disturb the core-region stream inside the blade due to the complicated channel shape. Inspired by the different turbulence promotion targets of ribs and wavy tapes, a two-pass ribbed cooling channel combined with wavy tape insert was proposed. It was expected that the ribs and wavy tapes

can complement each other in the cooling channel and achieve better cooling performance. The synergistic effect the combined near-wall and core-region heat transfer promoter was numerically studied. Two key geometrical factors, namely rib to wave crest phase shift and relative wave amplitude, have significant effect on the cooling performance. With optimal geometrical configuration, the combined cooling strategy can achieve significant heat transfer augment with relative low pressure-drop penalty. The flow detail illustration demonstrated that the secondary flow induced by wavy tape, which enhances the fluid mixing between near-wall and core-region, is responsible for the cooling performance improvement.

Numerical methodology

Geometry of the problem

Figure 1 shows the design of the two-pass cooling channel with ribs and wavy tape insert. The channel has a square cross-section with a side length of Each pass is about 61 cm long with an L/D ratio of 12. The distance between ribs is indicated by P , which is termed as rib pitch in this work. The rib height-to-channel width, e/D , and the pitch-to-height ratio, P/e , is 0.125 and 10. One 90° rib is placed along the divider wall in the middle of the 180° turn and nine 90° ribs are arranged in each pass in equal pitch.

As shown in fig. 1, a sinusoidal wavy tape is placed in the channel. Figure 2 presents the schematic of wavy tape configurations and the definition of important geometric parameters. The variation of the height of the wavy tape, h , with streamwise distance x can be expressed:

$$h = A \sin\left(2\pi \frac{x}{P} + \varphi\right) \quad (1)$$

where φ is the phase shift between wavy tape and rib. Four different phase shifts were studied, namely 0° , 90° , 180° , and 270° . In case of $\varphi = 0^\circ$ phase shift, the rib top and wave peak are in-line with each other. At the other extreme, the $\varphi = 180^\circ$ phase shift corresponds to exactly one half wavelength, the rib top and wave trough are in-line. The following reduced parameters are used to characterize geometry in channel with sinusoidal wavy tape: phase shift, φ , and relative wave amplitude, A/e .

Data reduction

The goal of this study is to investigate the local heat transfer rate and pressure drop for ribbed channels with wavy tape insert. The heat transfer coefficient is defined:

$$h = \frac{q}{T_w - T_b} \quad (2)$$

where q is the heat flux, T_w – the wall temperature, and T_b – the bulk mean temperature of flow.

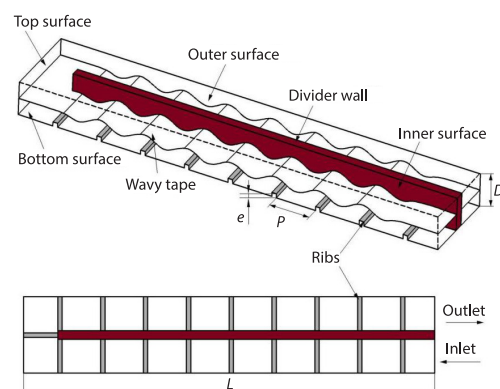


Figure 1. Geometry of the two-pass ribbed channel with wavy tape inserts

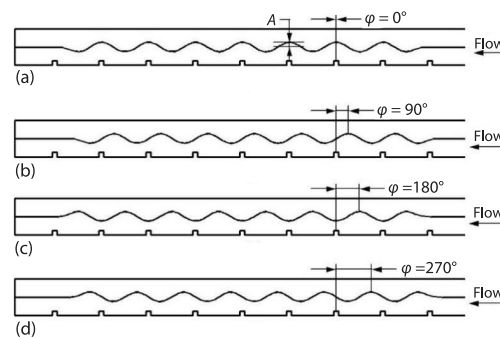


Figure 2. Schematic of wavy tape configurations and definition of geometric parameters; (a) $\varphi = 0^\circ$, (b) $\varphi = 90^\circ$, (c) $\varphi = 180^\circ$, and (d) $\varphi = 270^\circ$

The Reynolds number based on the channel width is given:

$$\text{Re} = \frac{\rho U D}{\mu} \quad (3)$$

where ρ is the density of air, U – the inlet air velocity, and μ – the dynamic viscosity of air.

Nusselt number is defined:

$$\text{Nu} = \frac{hD}{k} \quad (4)$$

where h is the heat transfer coefficient and k – the thermal conductivity of air.

The Nusselt numbers presented in this paper were normalized with a smooth channel correlation, Kays [31], for fully developed, stationary, turbulent flow:

$$\text{Nu}_0 = 0.023 \text{Re}^{0.8} \text{Pr}^{0.4} \quad (5)$$

where Pr is the Prandtl number of air. In fully developed channel flow, the friction factor can be determined by the pressure drop across the flow duct and the inlet velocity, and is evaluated:

$$f = \frac{2}{D} \frac{\Delta P}{L \rho U^2} \quad (6)$$

The friction factors are normalized by the friction factor for fully developed turbulent flow in two-pass ribbed channel with flat tape insert, which is defined as f_0 . With Nusselt number and friction factor ratios, the overall thermal performance, TP , is defined:

$$TP = \frac{\frac{\text{Nu}}{\text{Nu}_0}}{\left(\frac{f}{f_0}\right)^{1/3}} \quad (7)$$

Numerical model

Boundary conditions: Air was applied as the working fluid in all cases with constant inlet velocity, uniform inlet temperature (323.15 K, $\text{Pr} = 0.7$), and constant outlet pressure (1 atmosphere). No-slip wall conditions were implemented over all walls. The temperature of the bottom surface and ribs was maintained constant at 330 K while the other walls were assumed as adiabatic wall condition. The Reynolds number based on the channel width is ranged from 6000-30000.

Grid generation: The square channel domain was divided into two smaller domains by the wavy tape. These two domains can be calculated independently as there is no mass and heat transfer (by assumption) between the two domains. This study only considered the domain with ribs. The grid of the computational domain was generated with the computer tool ICEM. The generated grid was quadrilateral with regular grid elements. The total element numbers of the two-pass channel were about $1000 \times 45 \times 40$ (length, width, and height).

Mathematical formulation and governing equations: The 3-D and incompressible Navier-Stokes equations were solved with software FLUENT. The flow through the channel was governed by the RANS eqs. (8) and (9) and the energy eq. (10):

$$\frac{\partial}{\partial x_i}(\rho u_i) = 0 \tag{8}$$

$$\frac{\partial}{\partial x_i}(\rho u_i u_j) = \frac{\partial}{\partial x_i} \left[\mu \left(\frac{\partial u_i}{\partial x_j} - \overline{\rho u_i' u_j'} \right) \right] - \frac{\partial P}{\partial x_i} \tag{9}$$

$$\frac{\partial}{\partial x_i}(\rho u_i T) = \frac{\partial}{\partial x_i} \left((\Gamma + \Gamma_t) \frac{\partial T}{\partial x_j} \right) \tag{10}$$

where Γ is the molecular thermal diffusivity and Γ_t – the turbulent thermal diffusivity.

The standard $k-\epsilon$ model with scalable wall function was adopted as turbulence model. The pressure gradient in the momentum equation was evaluated with the coupled algorithm. The differential equations were discretized with the second order upwind scheme. Default under-relaxation factors of the solver were used to control the update of computed variables at each iteration. A convergence criterion of 10^{-5} was used for the maximum error RMSE in all cases. A typical case consumed around 5 hours and 8 Intel Xeon E5-2640 v4 CPU to run about 700 iterations.

Grid independence verification and validation: The effect of grid size was analyzed by comparing the regionally averaged Nusselt number computed for grids with five different refinement degrees. Two tests were conducted to determine the grid resolution in the cross-stream and streamwise directions, respectively. As shown in fig. 3(a), in the first test, three grid configurations $1000 \times 35 \times 30$, $1000 \times 45 \times 40$ and $1000 \times 60 \times 55$ (1000 cells in the streamwise direction and 35×30 , 45×40 , 60×55 cells in two cross-stream directions) were evaluated. The improvement in the regionally averaged Nusselt number ratio is 1.62% as numerical grid is refined from $1000 \times 35 \times 30$ to $1000 \times 45 \times 40$. Further grid refinement to $1000 \times 60 \times 55$ provides only 0.03 percent improvement for regionally averaged Nusselt number ratio. In the second test, three grid configurations $700 \times 45 \times 40$, $1000 \times 45 \times 40$ and $1500 \times 45 \times 40$ were evaluated to determine the grid resolution in the streamwise direction. 0.2 percent and 0.1 percent improvements are produced as numerical grid is refined from $700 \times 45 \times 40$ to $1000 \times 45 \times 40$ and further to $1500 \times 45 \times 40$. The grid independence tests indicate that the Nusselt number is more sensitive to the grid resolution in the cross-stream direction than in the streamline direction. The final adopted hexahedron grid is shown in fig. 3(b).

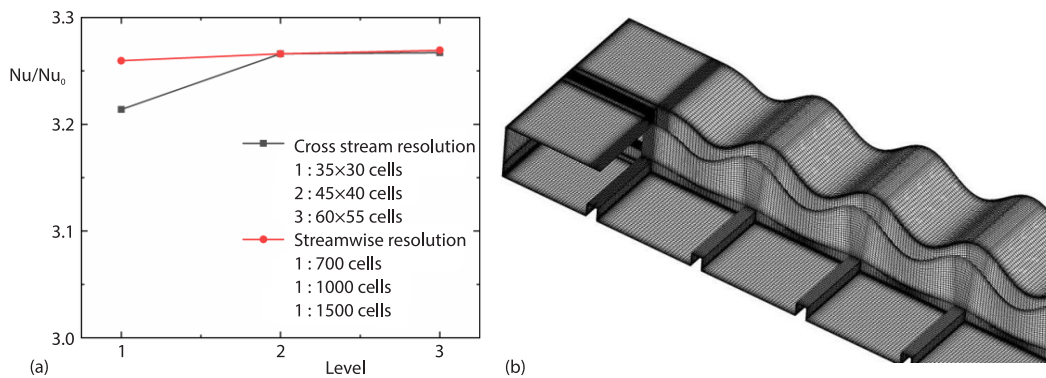


Figure 3. Grid independence investigation (a) and adapted grid detail (b)

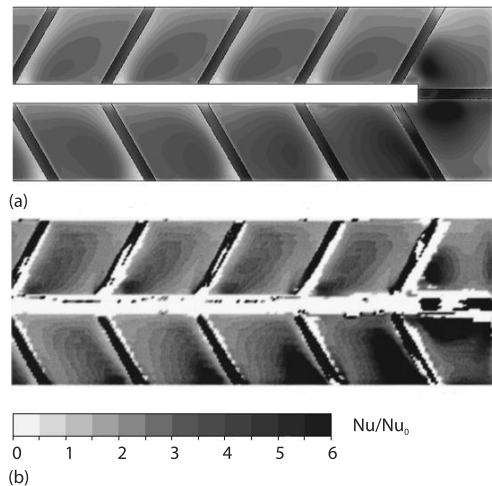


Figure 4. Detailed Nusselt number ratio distributions for 60° angled ribbed channel: (a) numerical result and (b) experimental result [32], $Re = 30000$

To validate the numerical method, the results of this study were compared with experimental data of Ekkad and Han [32]. Figure 4 depicts the Nusselt number ratio contour plots on the bottom surfaces in a two-pass ribbed channel without tape insert at $Re = 30000$. The numerical model kept same channel and rib dimensions, working fluid, and similar flow condition (Reynolds number, inlet temperature) with the experimental rig. The experimental Nusselt number ratios were obtained from thermochromic liquid crystals, which reflected the temperature on the tested surface. Combined with the initial temperature of the tested surface and the oncoming time-dependent mainstream temperature, the heat transfer coefficient and Nusselt number were calculated. Periodic heat transfer distributions are obtained in both passages. The highest Nusselt number ratios appear on the top of ribs, last corner in the first

passage, first corner in the second passage and downstream of the 90° rib. Numerical results show a good agreement with the experimental distribution of Nusselt number ratio.

Results and discussion

Comparison of flat tape and wavy tapes with different amplitudes

The detailed Nusselt number ratio distributions of flat tape and wavy tapes with different amplitudes for $\varphi = 0^\circ$ configuration at $Re = 15500$ are drawn in figs. 5(a)-5(e). It can be observed that the flat tape has the lowest Nusselt number ratio and larger wave amplitude leads to larger Nusselt number ratio and significant difference in the location of higher heat transfer areas (HHTA). The HHTA are found on center areas between adjacent ribs in cases of flat tape and wavy tapes with small relative wavy amplitude. As wave amplitude increases, HHTA move to the sides near the inner and outer wall between adjacent ribs. To explain this phenomenon, fig. 5(f) displays the velocity vectors along one bottom surface between ribs in case of $A/e = 1.5$ at $Re = 15500$. Fluid is transported from the center to around as denoted in circles. It can be inferred that the fluid reattach the bottom surface near the two circles after the separation induced by the rib. The wave amplitude will affect the reattachment of the flow. In the case of this study, as the wave amplitude increases the reattachment moves from the center area between two ribs to the area near corners after the ribs.

Figure 6 presents the spanwise averaged Nusselt number distributions for four different wave amplitude configurations at $Re = 15500$. It seems that wavy tape mainly affects the amplitude of Nusselt number and has little effect on the distribution of Nusselt number except for $A/e = 2.0$. The number of peaks Nusselt number for $A/e = 2.0$, denoted by the enlarged area, is different from others. Two peaks indicate more uniform Nusselt number distribution compared to one peak. Overall, the Nusselt number ratio between ribs increases with the relative wave amplitude and the distribution does not change much. The relative wave amplitude has the greater effect on the Nusselt number ratio on the regions between ribs compared to the regions on the tops.

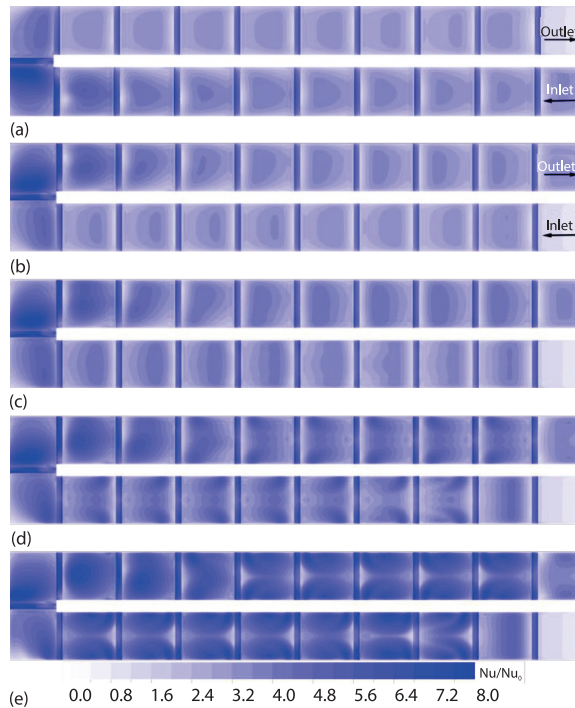


Figure 5. Detailed Nusselt number ratio distributions for $\phi = 0$ configuration at $Re = 15500$ in a two-pass ribbed channel; (a) flat tape, (b) $A/e = 0.5$, (c) $A/e = 1.0$, (d) $A/e = 1.5$, (e) $A/e = 2.0$, and (f) velocity vectors along bottom surface for $A/e = 1.5$

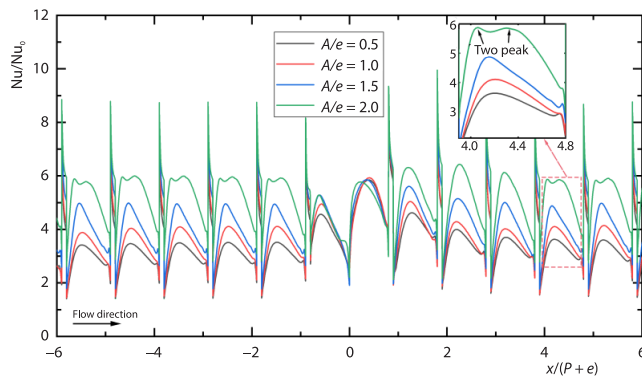


Figure 6. Spanwise averaged Nusselt number distributions at $Re = 15500$; one bottom surface between ribs is picked to enlarge and illustrate the two peaks Nusselt number of $A/e = 2.0$

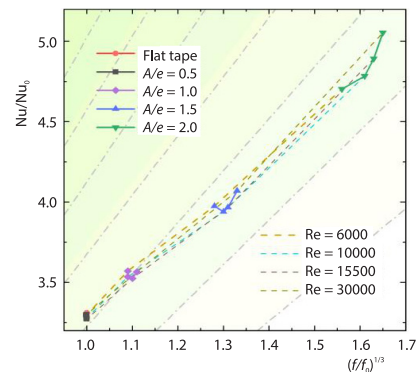


Figure 7. Average Nusselt number ratio vs. average friction factor ratio for four wavy amplitude configurations; deeper background indicates larger thermal performance

The overall thermal performance for different wave amplitude configurations over a range of studied Reynolds numbers are compared in fig. 7. Larger Reynolds number always lead to larger friction factor. However, the trends of Nusselt number ratio, Nu/Nu_0 , with Reynolds number for different wave amplitude are distinctly different. The Nu/Nu_0 for $A/e = 1.0$ and 1.5 decrease at first and then increase with increasing Reynolds number, while the Nu/Nu_0 for $A/e = 2$ always increases. The overall thermal performance decreases with increasing wave amplitude. The 0.5 time relative wave amplitude has very little effect on Nu/Nu_0 and friction factor, $(f/f_0)^{1/3}$. The corresponding augments are 1.43 - 1.53 times and 1.56 - 1.65 times for the case

of $A/e = 2$. The results illustrate that the smaller wave amplitude achieves relative better overall thermal performance without compromising much pressure-drop penalty. The larger wave amplitude gains greater heat transfer coefficient, while leading to higher pressure drop.

Effect of phase shift

The phase shift determines the variation of flow sectional area, which will lead to different averaged main flow velocity distribution and thus Nusselt distribution. Figure 8 presents the detailed Nusselt number ratio distributions in the two-pass channel at $Re = 15500$ for different phase shifts. Streamwise and axial variations are significant in the Nusselt number ratio distributions due to the ribs. Highest Nusselt number ratios appear on the top of the ribs. Nusselt number ratios are very low immediately before and after the ribs. In case of

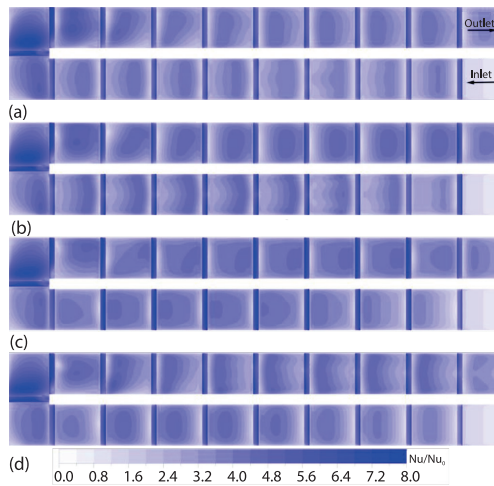


Figure 8. Detailed Nusselt number ratio distributions for $A/e = 1$ configuration at $Re = 15500$; (a) $\varphi = 0^\circ$, (b) $\varphi = 90^\circ$, (c) $\varphi = 180^\circ$ and (d) $\varphi = 270^\circ$

of $\varphi = 0^\circ$, heat transfer is higher in the middle region between two ribs. In case of $\varphi = 90^\circ$, higher heat transfer is observed after ribs in the first passage and before ribs in the second passage. The opposite occurs in case of $\varphi = 270^\circ$. In case of $\varphi = 180^\circ$, heat transfer is higher before ribs in both passages. As referred by Liu and Wang [10], the added ribs can cause some lower heat transfer areas (LHTA). Compared to the case of $\varphi = 0^\circ$, the before-rib LHTA in second passage are eliminated by wavy tape with $\varphi = 90^\circ$. The before-rib LHTA in first passage are eliminated by wavy tape with $\varphi = 270^\circ$. Both before-rib LHTA in first passage and second passage are eliminated by wavy tape with $\varphi = 180^\circ$. In general, the position of HHTA can be adjusted to eliminate some LHTA with wavy tape of different phase shift. Wavy tape of $\varphi = 180^\circ$ can produce more uniform heat transfer distribution than others, which can be confirmed by the spanwise averaged Nusselt number ratio distributions.

The spanwise averaged Nusselt number ratio distributions for four different phase shift configurations at $Re = 15500$ are compared in fig. 9. As the 90° ribs are along the channel

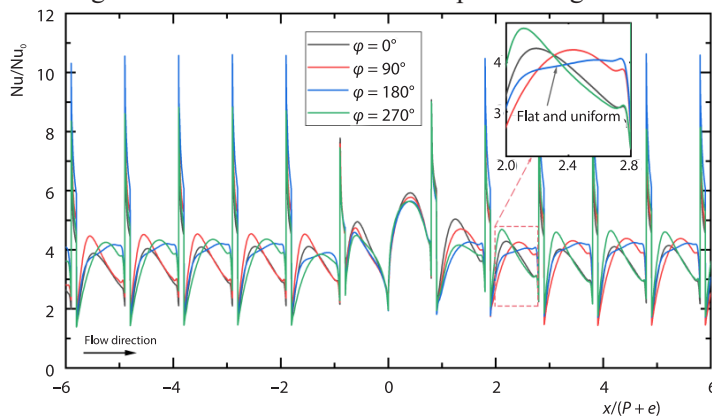


Figure 9. Spanwise averaged Nusselt number distributions at $Re = 15500$; one bottom surface between ribs is picked to enlarge and illustrate the Nu distribution of $\varphi = 180^\circ$

span, the averaging is also along the span. Periodic spikes are found in the spanwise averaged distributions, which indicates the presence and position of the ribs. The bottom distribution of Nusselt number ratio for $\varphi = 180^\circ$ is more uniform compared to other three as shown in the enlarged area. The highest Nusselt number can reach to around 10 on the top of ribs and reach to 4 for regions between two adjacent ribs.

For sake of quantitative evaluation, fig. 10 provides the Nusselt number ratio vs. the reduced friction factor ratio for four phase shift configurations over varied Reynolds number. The results indicate that the increasing Reynolds number leads to larger friction factor ratio for all four phase shift configurations. Moreover, increasing Reynolds number also results in lower Nusselt number ratio until Reynolds number of 15500. Overall, heat transfer performance decreases with increasing Reynolds number. Among different phase shifts, 180° phase shift achieves the largest heat transfer enhancement compared to other three. The 180° phase shift obtains 1.18-1.19 times the flat tape heat transfer enhancement with 1.32-1.35 times the pressure drop penalty. As for the overall thermal performance, 0° phase shift does best. The 0° phase shift achieves 1.07-1.08 times heat transfer enhancement with only 1.09-1.11 times the pressure drop penalty. It can be concluded that the 0° phase shift provides best overall thermal performance, while the 180° phase shift gains greatest Nusselt number.

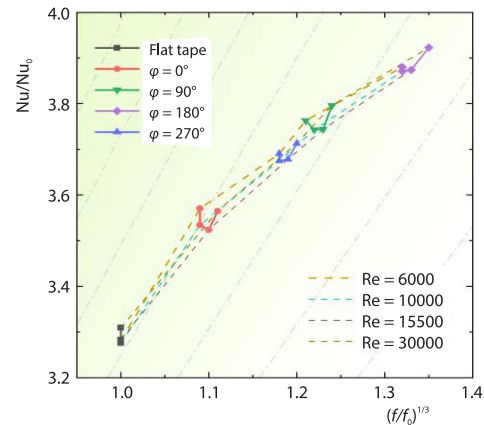


Figure 10. Average Nusselt number ratio vs. reduced friction factor ratio for four phase shift configurations; deeper background indicates larger thermal performance

Performance improvement mechanism of wavy tape

To illustrate the performance improvement mechanism of wavy tape, figs. 11(a) and 11(b) compare the detailed Nusselt number ratio distributions for the channels with typical wavy tape and flat tape at $Re = 15500$. Obviously, heat transfer is enhanced in case of wavy tape compared to flat tape. To illustrate the effect of wavy tape, the Nusselt number distribution

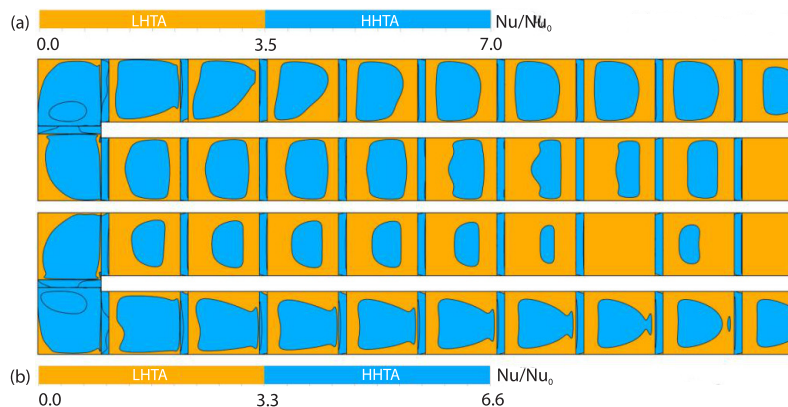


Figure 11. Detailed Nusselt number ratio distributions for the ribbed channel at $Re = 15500$; (a) wavy tape, $A/e = 1.0$ and (b) flat tape

was divided to two contrary parts: LHTA and HHTA. The areas with Nusselt number ratio lower than average are defined as LHTA, while the areas with Nusselt number ratio higher than average are defined as HHTA. The enhancement occurred in the center areas between ribs in the first and second passage. Noted that the shape of the HHTA between ribs for the two cases are markedly different. The HHTA between ribs for flap tape reach one rib in the first pass and cannot reach any ribs or side walls in the second pass, whereas those for wavy tape can reach two side walls all the way. The wavy tape can eliminate the LHTA near the side walls, which can explain the larger averaged Nusselt number of wavy tape. What's more, the Nusselt number ratio is much higher in the first pass than that of the second pass for flat tape. Obviously, the Nusselt number ratio is more uniformly distributed in case of wavy tape, which is beneficial to produce more uniform temperature distribution.

To examine how the LHTA are eliminated, two cross-sections were chosen to display the velocity vectors in the two cases. As shown in fig. 12, Section I is placed between two ribs along the flow direction and Section II is placed on the top of one rib. From Section I of fig. 12(b), it can be observed that core-region fluid is transported to near-wall area along inner and outer side walls. Meanwhile, near-wall fluid is transported to core-region area and two vortices raise in the corners under the tape, which is shown in Section II of fig. 12(b). Figure 12(b) displays the secondary flow patterns in the ribbed channel with wavy tape insert. Core-region fluid transfers into near-wall region between the ribs and near-wall fluid then transfers back into the core region on the top of ribs, which forms periodic mass transfer in the channel with wavy tape insert. However, secondary flow cannot be found in fig. 12(a) at same positions in case of flap tape. It can be concluded that secondary flow induced by wavy tape is responsible for the enhanced heat and mass transfer in ribbed channel.

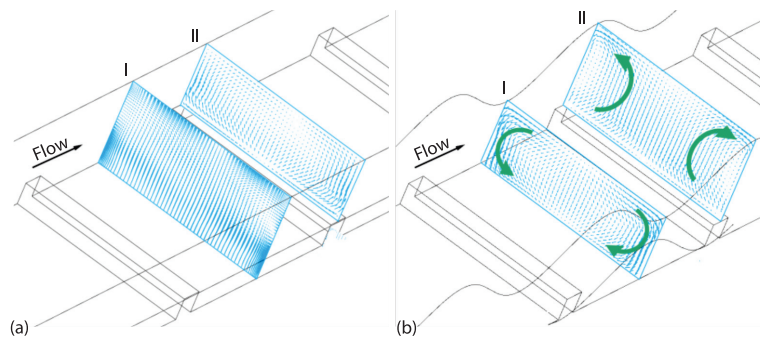


Figure 12. Velocity vectors along the cross-sections for a two-pass ribbed channel at $Re = 15500$; (a) flat tape and (b) wavy tape, $A/e = 1.0$, $\phi = 0^\circ$

Conclusions

A two-pass ribbed channel with wavy tape insert is proposed in this work. Numerical simulation has been carried out to investigate the effect of the sinusoidal wavy tape on the heat transfer distributions and pressure drop in a two-pass rectangular channel with one-side ribbed for Reynolds numbers from 6000-30000. The ribbed channel enhanced by wavy tape insert is targeting at augment the internal blade cooling performance of gas turbine. The obtained results can also be applied in some compact heat exchangers. The main results and findings of this study are summarized.

- The phase shift significantly affects the Nusselt number ratios distribution. 90° phase shift configuration can eliminate before-rib LHTA in second passage and 270° phase shift confi-

uration can eliminate before-rib LHTA in first passage. The 180° phase shift configuration can eliminate both before-rib LHTA in the first passage and the second passage. Besides, the 180° phase shift configuration provides more uniform Nusselt number ratio distribution between two adjacent ribs. In general, 0° phase shift achieves best overall thermal performance, which provides 1.07 to 1.08 times the flat tape heat transfer enhancement with 1.09-1.11 times the pressure drop penalty.

- The wave amplitude can change the position of the reattachment point. The reattachment point moves from the center area between two ribs to the area near corners as the wave amplitude increases. In this way, the wave amplitude can affect the Nusselt number ratio distribution. Smaller wave amplitude achieves relatively better overall thermal performance. To achieve obvious heat transfer augment, relative wave amplitude larger than 0.5 is required.
- With wavy tape insert in the channel, core-region fluid transfers into near-wall region between the ribs and near-wall fluid then transfers back into the core region on the top of ribs, which forms periodic mass transfer in the channel and eliminates the LHTA near the side walls. Therefore, it is the secondary flow induced by wavy tape that enhances the fluid mixing and augments the heat and mass transfer in ribbed channel.

Acknowledgment

This project has received funding from the China Postdoctoral Science Foundation under grant number 2020M672411, Natural Science Foundation of Hubei Province under grant number 2021CFB114 and National Natural Science Foundation of China under grant number U20A20303. The authors acknowledge the financial support by Youth Talent Promotion Project of Chinese Society of Electrical Engineering.

Nomenclature

A	– wave amplitude, [m]	Pr	– Prandtl number of air, [–]
D	– square channel width and height, [m]	q	– heat flux, [Wm^{-2}]
e	– rib height, [m]	Re	– Reynolds number, [–]
f	– friction factor, [–]	T_b	– bulk mean temperature of flow, [K]
f_0	– friction factor of channel with flat tape, [–]	T_w	– wall temperature, [K]
h	– heat transfer coefficient, [$Wm^{-2}K^{-1}$]	U	– mainstream flow velocity, [ms^{-1}]
k	– thermal conductivity of air, [$Wm^{-1}K^{-1}$]		
L	– length of the channel, [m]		
Nu	– local Nusselt number, [–]		
Nu_0	– Nusselt number from correlation for a straight channel, [–]		
P	– rib pitch, [m]		
ΔP	– pressure drop from inlet to outlet, [Pa]		

Greek symbols

μ	– dynamic viscosity of air, [Nsm^{-2}]
ρ	– density of air, [kgm^{-3}]
ϕ	– phase shift, [°]

References

- [1] Han, J., Heat Transfer and Friction in Channels with Two Opposite Rib-Roughened Walls, *Journal of heat Transfer*, 106 (1984), 4, pp. 774-781
- [2] Han, J., et al., Heat Transfer Enhancement in Channels with Turbulence Promoters, *Journal of Engineering for Gas Turbines and Power*, 107 (1985), 3, pp. 628-635
- [3] Han, J., Park, J. S., Developing Heat Transfer in Rectangular Channels with Rib Turbulators, *International Journal of Heat and Mass Transfer*, 31 (1988), 1, pp. 183-195
- [4] Han, J., et al., Augmented Heat Transfer in Rectangular Channels of Narrow Aspect Ratios with Rib Turbulators, *International Journal of Heat and Mass Transfer*, 32 (1989), 9, pp. 1619-1630
- [5] Chandra, P. R., et al., Effect of Rib Angle on Local Heat/Mass Transfer Distribution in a Two-Pass Rib-Roughened Channel, *Journal of Turbomachinery*, 110 (1988), 2, pp. 233-241
- [6] Han, J., et al., Local Heat/Mass Transfer Distributions Around Aharp 180 Deg Turns in Two-Pass Smooth and Rib-Roughened Channels, *Journal of Heat Transfer*, 110 (1988), 1, pp. 91-98

- [7] Chyu, M. K., Regional Heat Transfer in Two-Pass and Three-Pass Passages With 180 Deg Sharp Turns, *Journal of Heat Transfer*, 113 (1991), 1, pp. 63-70
- [8] Huh, M., et al., Effect of Rib Height on Heat Transfer in a Two Pass Rectangular channel (AR = 1: 4) with a Sharp Entrance at High Rotation Numbers, *International Journal of Heat and Mass Transfer*, 52 (2009), 19-20, pp. 4635-4649
- [9] Huh, M., et al., Influence of Channel Orientation on Heat Transfer in a Two-Pass Smooth and Ribbed Rectangular Channel (AR = 2: 1) under Large Rotation Numbers, *Journal of Turbomachinery*, 134 (2012), 1, 011022
- [10] Liu, H., Wang, J., Numerical Investigation on Synthetical Performances of Fluid-Flow and Heat Transfer of Semiattached Rib-Channels, *Int. J. of Heat and Mass Transfer*, 54 (2011), 1-3, pp. 575-583
- [11] Xie, G., et al., Turbulent Flow Characteristics and Heat Transfer Enhancement in a Square Channel with Various Crescent Ribs on one Wall, *Int. J. of Heat and Mass Transfer*, 115 (2017), Part A, pp. 283-295
- [12] Rana, J., et al., Computational Fluid Dynamics Analysis of a V-rib with Gap Roughened Solar Air Heater, *Thermal Science*, 22 (2018), 2, pp. 963-972
- [13] Li, Y., et al., Heat Transfer and Pressure Loss of Turbulent Flow in Channels with Miniature Structured Ribs on one Wall, *International Journal of Heat and Mass Transfer*, 131 (2019), Mar., pp. 584-593
- [14] Nine, M. J., et al., Turbulence and Pressure Drop Behaviors Around Semicircular Ribs in a Rectangular Channel, *Thermal Science*, 18 (2014), 2, pp. 419-430
- [15] Wang, G., et al., Fluid and Heat Transfer Characteristics of Micro-Channel Heat Sink with Truncated Rib on Sidewall, *International Journal of Heat and Mass Transfer*, 148 (2020), 119142
- [16] Sahel, D., et al., Effect of the Size of Graded Baffles on the Performance of Channel Heat Exchangers, *Thermal Science*, 24 (2020), 2A, pp. 767-775
- [17] Kreith, F., Margolis, D., Heat Transfer and Friction in Turbulent Vortex Flow, *Applied Scientific Research, Section A*, 8 (1959), 1, pp. 457-473
- [18] Promvong, P., Eiamsa-Ard, S., Heat Transfer Behaviors in a Tube with Combined Conical-Ring and Twisted-Tape Insert, *International Communications in Heat and Mass Transfer*, 34 (2007), 7, pp. 849-859
- [19] Bharadwaj, P., et al., Heat Transfer and Pressure Drop in a Spirally Grooved Tube with Twisted Tape Insert, *International Journal of Heat and Mass Transfer*, 52 (2009), 7-8, pp. 1938-1944
- [20] Chang, S. W., et al., Heat Transfer and Pressure Drop in Tube with Broken Twisted Tape Insert, *Experimental Thermal and Fluid Science*, 32 (2007), 2, pp. 489-501
- [21] Rush, T., et al., An Experimental Study of Flow and Heat Transfer in Sinusoidal Wavy Passages, *International Journal of Heat and Mass Transfer*, 42 (1999), 9, pp. 1541-1553
- [22] Kuhn, S., von Rohr, P. R., Experimental Investigation of Mixed Convective Flow over a Wavy Wall, *International Journal of Heat and Fluid-Flow*, 29 (2008), 1, pp. 94-106
- [23] Chang, S. W., et al., Heat Transfer and Pressure Drop in Furrowed Channels with Transverse and Skewed Sinusoidal Wavy Walls, *International Journal of Heat and Mass Transfer*, 52 (2009), 19-20, pp. 4592-4603
- [24] Gong, L., et al., Parametric Numerical Study of Flow and Heat Transfer in Micro-Channels with Wavy Walls, *Journal of Heat Transfer*, 133 (2011), 5, 051702
- [25] Sui, Y., et al., Direct Numerical Simulation of Fluid-Flow and Heat Transfer in Periodic Wavy Channels with Rectangular Cross-Sections, *Int. J. of Heat and Mass Transfer*, 55 (2012), 1-3, pp. 73-88
- [26] Zhu, X. W., et al., A Novel Wavy-Tape Insert Configuration for Pipe Heat Transfer Augmentation, *Energy Conversion and Management*, 127 (2016), Nov., pp. 140-148
- [27] Zhu, X. W., et al., Wavy-Tape Insert Designed for Managing Highly Concentrated Solar Energy on Absorber Tube of Parabolic trough Receiver, *Energy*, 141 (2017), Dec., pp. 1146-1155
- [28] Bhattacharyya, S., et al., Effect of Novel Short-Length Wavy-Tape Turbulators on Fluid-Flow and Heat Transfer: Experimental Study, *Experimental Heat Transfer*, 33 (2020), 4, pp. 335-354
- [29] Yu, C., et al., Numerical Study on Turbulent Heat Transfer Performance of a New Parallel-Flow Shell and Tube Heat Exchanger with Sinusoidal Wavy Tapes Using RSM Analysis, *Applied Thermal Eng.*, 150 (2019), Mar., pp. 875-887
- [30] Liang, Y., et al., Numerical Investigation of Heat Transfer and Flow Characteristics of Laminar Flow in a Tube with Center-Tapered Wavy-Tape Insert, *Applied Thermal Eng.*, 148 (2019), Feb., pp. 557-567
- [31] Kays, W. M., *Convective Heat and Mass Transfer*, Tata McGraw-Hill Education, New York, USA, 2011
- [32] Ekkad, S. V., Han, J.-C., Detailed Heat Transfer Distributions in Two-Pass Square Channels with Rib Turbulators, *International Journal of Heat and Mass Transfer*, 40 (1997), 11, pp. 2525-2537